ELSEVIER

Intermetallics 9 (2001) 1069–1078

Intermetallics

www.elsevier.com/locate/intermet

Microstructure control and tensile properties of three-phase alloys based on the $E2_1$ Co_3AlC and B2 CoAl

Yoshisato Kimura[a,*], Yoshinao Mishima[a], C.T. Liu[b]

[a]*Tokyo Institute of Technology, Materials Science and Engineering, 4259 Nagatsuta, Midori-ku, Yokohama 226-8502, Japan*
[b]*Oak Ridge National Laboratory, Metals and Ceramics Division, PO Box 2008, Oak Ridge, TN 37831-6115, USA*

Received 27 July 2001; accepted 18 September 2001

Abstract

To investigate tensile mechanical behavior, tensile tests were conducted at room temperature and 1273 K on three-phase alloys consisting of the $E2_1$ Co_3AlC, B2 CoAl and (Co) primary solid solution. The alloy containing a large volume fraction of $E2_1$ phase exhibits excellent ductility, exceeding 5% plastic strain at room temperature, while the alloy with a considerable amount of coarse B2 phase particles shows zero ductility. In this study, microstructure control was used to improve the ambient temperature ductility of the $E2_1$/B2/(Co) three-phase alloys. Hot forging and subsequent heat treatments were performed aiming at eliminating solidification defects and minimizing the heterogeneity of the as-cast microstructure. These thermomechanical treatments together with compositional control effectively improve the ductility of the $E2_1$/B2/(Co) three-phase alloys at ambient temperature and 1273 K.
© 2001 Elsevier Science Ltd. All rights reserved.

Keywords: A. Intermetallics, miscellaneous; B. Phase diagram; B. Yield stress; F. Mechanical testing; F. Microscopy

1. Introduction

The technology to conserve fossil fuel and to minimize the effect of burning of fossil fuels on the global environment demands the development of heat resistant alloys that can operate at higher temperatures for maximum efficiency. In view of this, a great deal of effort has been devoted to developing new alloys based on intermetallic compounds for high temperature structural applications. The important strategy of alloy design based on intermetallic compounds involves not only how to overcome the extreme brittleness of intermetallic compounds but also how to achieve a good balance between strength and ductility that conflict with each other in most cases. From the viewpoint of plastic deformability of intermetallic compounds, the crystal structure should be as simple as possible to ensure sufficient operative slip systems and small Burgers vectors. A lot of intermetallic compounds have a simple crystal structure based on bcc, fcc and hcp; however, the formation of superlattice dislocations produces a large excess energy involving dislocation self energy and the anti-phase boundary energy associated with ordered structures. In most cases, intermetallic compounds are intrinsically brittle and limited plastic deformability can be obtained from the modification of their metallurgical and chemical properties of monolithic intermetallic compounds. Conventional metallurgy tells us that ductilizing is thought to be harder than strengthening materials. Therefore, we should first accomplish enough ambient temperature ductility prior to making a major effort on improving material strength at elevated temperatures. One of the methods to reduce the brittleness of intermetallic compounds is to introduce multi-phases including ductile disordered phase(s) [1,2]. The γ/γ' microstructure is the most successful example of multi-phase heat resistant alloys commercially used. The $L1_2$ Ni_3Al is a well-known strengthener in Ni-base superalloys [3–6]. The γ/α_2 lamellar microstructure of TiAl-based alloys is a good example to show that improvement of strength and ductility is possible through microstructure control of the brittle phases $L1_0$ TiAl and $D0_{19}$ Ti_3Al [7–9].

We have conducted a systematic investigation on the design of heat resistant alloys based on the $E2_1$ Co_3AlC and B2 CoAl ordered phases with or without primary solid solution (Co) in the Co–Al–C ternary system. A

* Corresponding author. Tel.: +81-45-924-5612; fax: +81-924-5495.

E-mail address: kimurays@materia.titech.ac.jp (Y. Kimura).

0966-9795/01/$ - see front matter © 2001 Elsevier Science Ltd. All rights reserved.
PII: S0966-9795(01)00113-3

series of investigations on this alloy design was originally initiated from the study of B2/(Co) two-phase alloys in the Co–Al binary system [10–13]. Our results indicate that neither ambient temperature ductility nor elevated temperature strength was sufficient in the B2/(Co) two-phase alloys. The study was thus extended to the Co–Al–Ni(-Ti) and Co–Al–C ternary alloy system. The $L1_2$ type $(Ni,Co)_3(Al,(Ti))$ is available in the former system [12–14], and the $E2_1$ type Co_3AlC co-exists with B2 and (Co) in the latter system [13,15–19]. The ordered crystal structures of $E2_1$ and $L1_2$ are quite similar to each other as mentioned later.

The phase diagram information of the Co–Al–C ternary system and microstructures of the alloys were first reported by Huetter et al. to the authors' best knowledge [20,21]. Several isotherms, isopleths and the reaction scheme of the Co–Al–C ternary system for the Co-rich portion were evaluated and revised by the present author as fundamental information of the phase equilibria among the $E2_1$ Co_3AlC, B2 CoAl and (Co) primary solid solution [13,17]. The isotherm of the Co–Al–C ternary system for the Co corner at 1373 K is shown in Fig. 1(a). The $E2_1$ Co_3AlC phase yields, through the ternary peritectic type invariant reaction, "liquid + C (graphite) + B2 CoAl + $E2_1$ Co_3AlC" at 1652 K [13,17]. Thus, the phase stability of the $E2_1$ Co_3AlC phase is almost the same as the $L1_2$ Ni_3Al of which the peritectic reaction temperature is 1658 K [22]. The $E2_1$ Co_3AlC

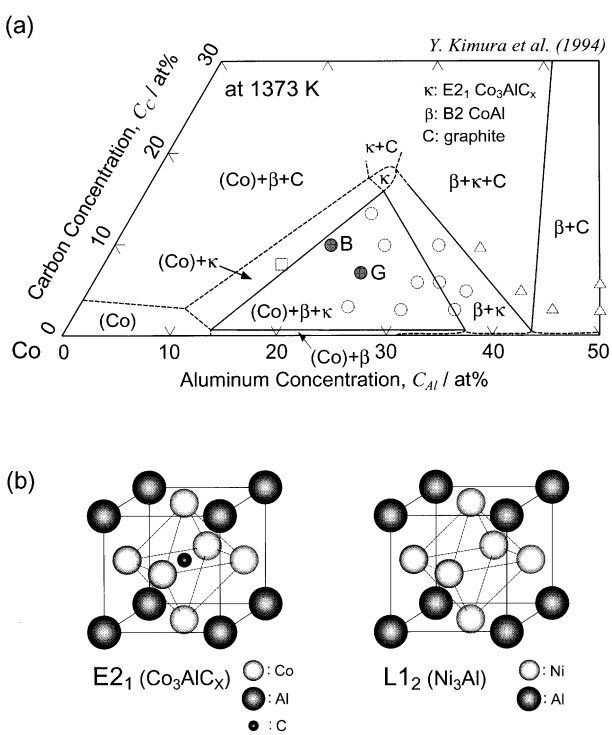

Fig. 1. Published phase diagram information: (a) the isotherm of the Co-corner of the Co–Al–C ternary system at 1373 K evaluated by the present authors [17], and (b) unit cells of the $L1_2$ and $E2_1$ crystal structures.

single phase field seems to be situated at less carbon content than the stoichiometric composition, 20 at.% C, since the solubility of C is restricted by the excess energy due to the interstitial elastic strain. Thus it is written in a formula Co_3AlC_x, where x is less than 1 [17,20,21]. Hwang et al. has clarified by a transmission electron microscopic (TEM) study that there exists extra long range ordering of carbon atoms in the Co_3AlC_x phase, by which x is evaluated as 0.5 [23,24]. Recently, Hosoda et al. reported that the $E2_1$ (or $L1_2$) compound, T_3AlC, where T stands for the 3rd period of transition metals (Cr, Mn, Fe, Co, Ni and Cu) may form a continuous solid solution throughout these T–Al–C systems [25]. It suggests that the design of alloys based on the $E2_1$ type intermetallic compound can systematically be conducted in a quite wide compositional range.

The $E2_1$ type ordered crystal structure is based on the $L1_2$ structure. An interstitial element C is ordered at the body center site, which is the octahedral interstitial site facing all six Co atoms of the $L1_2$ structure, as shown in Fig. 1(b). Since "the Co_3Al phase" is absent in the Co–Al binary system, the fcc-base $E2_1$ ordered structure is thought to be stabilized by an interstitial element [26,27]. In other alloy systems, we can find a lot of examples that the $E2_1$ phase is stabilized. The $E2_1$ Fe_3AlC is stable in the Fe–Al–C ternary system while the bcc-based $D0_3$ Fe_3Al exists in the Fe–Al binary system [28–33]. The V_3AuX (X = C, N, O) exists against complicated fcc-base A15 V_3Au [34,35] and $Ti_3AlC(N)$ against hcp-base $D0_{19}$ [36,37].

It is well-known from the literature that Ni_3Al and other $L1_2$ compounds exhibit the anomalous positive temperature dependence of strength, which can be an advantage for elevated temperature strength [38–44]. The same positive temperature dependence of strength observed in the $L1_2$ compounds is expected to appear in the $E2_1$ compounds as well because of the crystal structure similarity. Interstitial elements may contribute an additional strengthening effect at relatively low temperatures. Hosoda et al. [15,16] and two of the present authors [18,19] have investigated compressive mechanical behavior of the Co–Al–C ternary multi-phase alloys B2/$E2_1$/(Co). Compression tests conducted in a wide temperature range between 77 and 1273 K revealed the existence of a temperature region where a positive temperature dependence of strength appears for some Co–Al–C ternary alloys, though it is the result of the mixed contribution of constituent phases. Hwang et al. determined the operative slip system in the $E2_1$ phase by TEM work done on an $E2_1$/(Co) two-phase alloy deformed in compression [23,24]. The slip plane is {111} and Burgers vector **b** is <011>, all of which are the same for $L1_2$ compounds such as Ni_3Al [6,38–44].

The $E2_1$ Co_3AlC phase would be an attractive strengthener of a new class of Co-based heat resistant alloys. The objective of the present work is to investigate

tensile mechanical properties of the Co–Al–C ternary $E2_1$/B2/(Co) three-phase alloys, with the final goal to evaluate the potential of these alloys for high temperature structural application. Our interest is especially focused on the ambient temperature ductility improvement by means of the microstructure control. A specific heat treatment combined with hot forging was proposed in this work for the further improvement of ambient temperature ductility of the Co–Al–C ternary $E2_1$/B2/(Co) three-phase alloys through microstructural control and elimination of solidification defects and heterogeneity of the as-cast microstructure dominated by coarse dendrites.

2. Experimental procedures

The three-phase B2/$E2_1$/(Co) Co–Al–C ternary alloys were prepared by arc-melting under an argon gas atmosphere using raw materials with the highest purity readily available. The chemical compositions of alloys in Table 1 are represented on the isotherm at 1373 K of the Co–Al–C ternary system in Fig. 1 [17]. We used the same notation for the present alloys as used in our previous papers [17,19]. Symbols with a dotted line represent nominal compositions of the rest of the alloys prepared in this series of work. Wet chemical analysis was performed on alloy G. Annealing heat treatments were conducted at 1373 K for 108 ks (30 h) under a flowing argon gas atmosphere.

Tensile mechanical behavior was investigated on the selective alloys B and G which exhibit excellent compressive ductility showing virtually unlimited plastic strain as we reported previously [19]. Tensile tests were conducted at room temperature in air and at 1273 K in vacuum (10^{-4} Pa) using an Instron-type universal mechanical testing machine. The nominal initial strain rate was 1.1 or 3.3×10^{-3} s^{-1}. Tensile test specimens, having the dimension shown in Fig. 2 were prepared by using an electrically discharged cutting machine. Specimens were mechanically polished and then electrically polished in a 10% perchloric acid–methanol solution to remove the damaged surface layer prior to the tests. Microstructural observations were performed by means of optical microscopy (OM) and scanning electron microscopy (SEM). Specimens for OM were chemically etched in aqua regia after mechanical polishing. Fracture surfaces were observed by SEM fractographs to characterize the fracture manner of the alloys. In addition, the specimen surface near the fracture section of alloy B was examined by using SEM back scattered electron imaging (BEI) and elements mapping using energy dispersive spectroscopy (EDS) and wave-length dispersive spectroscopy (WDS).

We proposed a specific microstructural control for the further improvement of ambient temperature ductility and toughness of alloys B and G through hot forging combined with heat treatments, aimed at eliminating solidification defects and diminishing inhomogeneous as-cast microstructures. The profile of the heat treatment sequence taken in this work is shown in Fig. 3: hot forging at 1373 K in air, then holding at 1473 K for 1.2 ks (20 min) under an argon gas flow, followed by oil quenching, and finally holding at 1373 K for 86.4 ks (24 h) followed by air cooling in an argon gas atmosphere.

Table 1
Alloy compositions of alloys B and G

Alloys	Compositions (at.%)		
	Co	Al	C
B	70.0	20.0	10.0
G[a]	68.75	24.23	7.02

[a] Results of wet chemical analysis.

3. Results and discussion

3.1. Tensile properties of as-annealed B2/$E2_1$/(Co) alloys

3.1.1. Microstructural features

Typical optical micrographs of alloy B (70Co–20Al–10C; nominal, at.%) and alloy G (68.75Co–24.23Al–

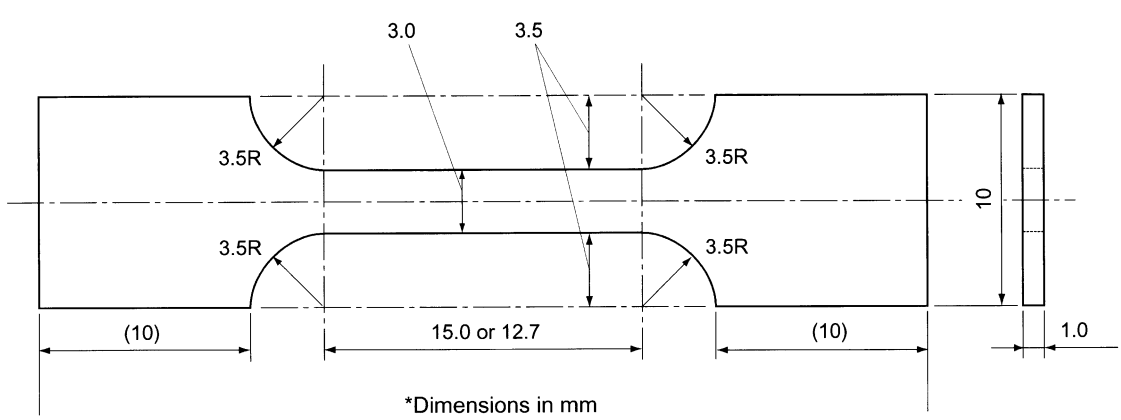

Fig. 2. The dimensions of a tensile test specimen in mm.

7.02C; wet chemically analyzed, at.%) in the annealed cast condition are presented in Fig. 4(a) and (b). They have the three-phase microstructure consisting of B2 CoAl, $E2_1$ Co_3AlC and primary solid solution (Co), in which the B2 CoAl phase is seen in light gray contrast, $E2_1$ Co_3AlC phase in dark gray contrast, and (Co) phase in white contrast. Note that the characterization of the various kinds of microstructures is explained in detail for the Co–Al–C ternary alloys, including alloys B and G, in our previous papers [17]. Essentials of alloys B and G are summarized as follows.

Alloys B and G have different microstructural features as characterized by the volume fractions of constituent phases as well as the solidification sequence, though they have the matrix composed of an eutectic microstructure of $E2_1$ and (Co) in common. The volume fractions of constituent phases, B2:$E2_1$:(Co), is roughly estimated as 6:52:42 in alloy B and 30:34:36 in alloy G. The primary solidifying phase is $E2_1$ Co_3AlC in alloy B and B2 CoAl in alloy G. The morphology of $E2_1$ Co_3AlC can be categorized in two distinctive configurations: one is coarse dendrites and the other is a part of the eutectic product with (Co). Coarse $E2_1$ phase dendrites dominate the microstructures of alloys B and G. The distinctive feature of alloy G is the existence of the primary solidifying coarse B2 phase dendrites and particles, which distinguishes it from alloy B. The microstructure of alloy B is differentiated by a substantial amount of coarse $E2_1$ phase dendrites and the $E2_1$/(Co) eutectic matrix. A very small volume fraction of B2 phase in fine particle sizes exists as well in alloy B.

3.1.2. Tensile properties

Tensile tests were conducted first at room temperature on the selected B2/$E2_1$/(Co) three-phase alloys B and G, which exhibited excellent compressive ductility showing virtually unlimited plastic deformation at room temperature and even at 77 K. Stress–strain curves obtained from tensile tests are shown in Fig. 5 together with those from the compression tests.

It is interesting to compare mechanical behaviors in compression and in tension. Room temperature tensile ductility is completely different in alloys B and G, even though the excellent compressive ductility looks totally the same in both alloys. It must be emphasized that the alloy B exhibits good tensile ductility reaching over 5.2%

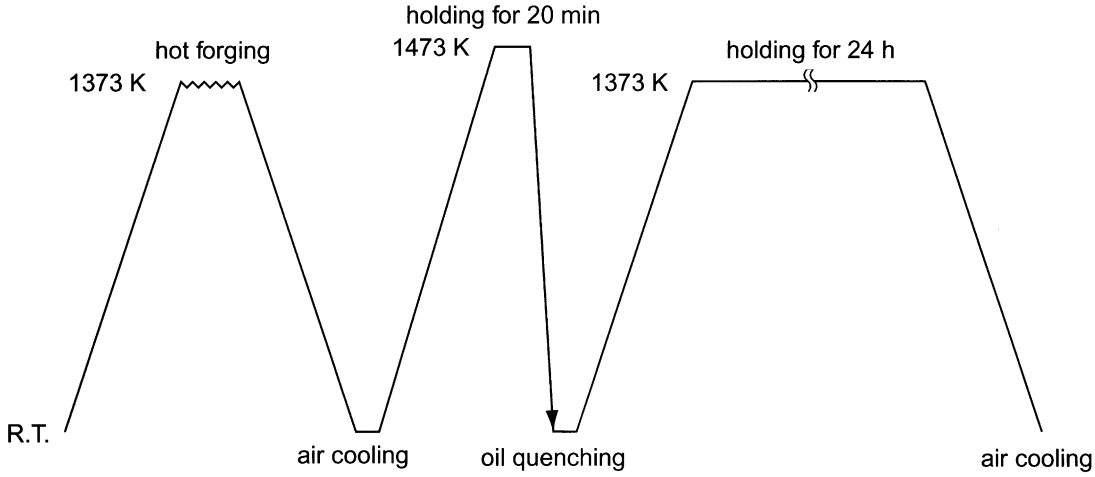

Fig. 3. A chart of the specific heat treatment sequence proposed in this work.

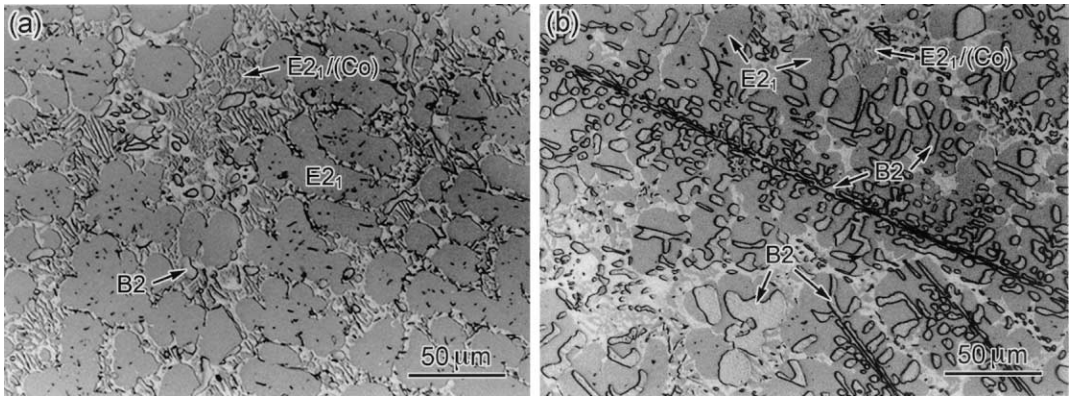

Fig. 4. Optical micrographs showing typical microstructures of as-annealed alloys: (a) alloy B and (b) alloy G.

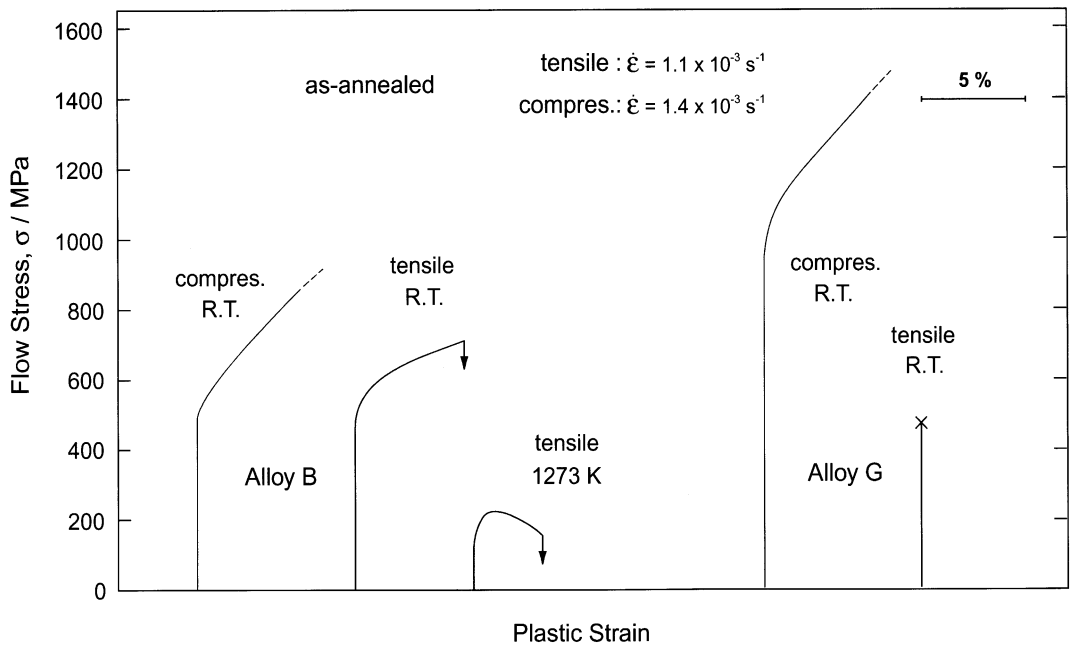

Fig. 5. Stress–strain curves obtained from tensile tests of as-annealed alloys B and G compared with those from compression tests.

plastic strain at room temperature. Well-developed steps on the surface of the tensile fractured specimen are clearly visible even with a naked eye, indicating a substantial amount of plastic deformation prior to fracture. Judging from the microstructure, coarse $E2_1$ phase dendrites and the $E2_1$/(Co) eutectic microstructure contribute to the plastic deformation at room temperature. On the contrary, alloy G fractures catastrophically in tension within elastic region before the onset of yielding, despite its excellent compressive ductility. It is predicted that coarse B2 phase dendrites and particles would be the cause of zero ductility. The yield strength defined by 0.2% tensile flow stress of alloy B is 463 MPa, which is comparable to that of the compressive strength of 530 MPa. The tensile fracture stress of alloy G in the elastic region is about 480 MPa, almost half the value of the compressive 0.2% flow stress, indicating high brittleness of alloy G.

A tensile test at 1273 K was conducted on alloy B, of which the stress–strain curve is shown in Fig. 5. Alloy B was found to be less ductile (3.2%) at 1273 K than at room temperature. This unusual temperature dependence of ductility is reproducible, and its cause is not well understood at the present time. Solidification defects as shown in Fig. 6(c) are expected to reduce tensile ductility at 1273 K but can not explain the decrease in ductility from room temperature to 1273 K. The tensile yield strength at 1273 K is about 150 MPa, which is much lower than that of 350 MPa reported previously in compression.

3.1.3. Fracture behavior

Fig. 6(a) and (b) shows typical SEM fractographs of alloys B and G tested at room temperature. It is apparent that the fracture takes place via an extremely brittle manner in alloy G, while the ductile fracture surface of alloy B indicates prominent plasticity of the alloy. In the case of alloy G, relatively large facets with smooth surfaces seen in the fractograph are supposed to be solidification defects at B2 phase dendrites or/and $E2_1$ phase dendrites. These defects induce phase separation and/or severe cracking which lead to catastrophic failure. Transgranular cleavage facets are also found in both alloys B and G, and the facet size varies widely. On comparison of the fractographs with the optical micrographs in Fig. 4, these cleavage facets seem to coincide with B2 phase dendrites.

As a further investigation to determine the fracture manner in alloy B, sub-cracks near the fracture surface were examined. A typical BEI taken from the vicinity of the fracture surface of alloy B is shown in Fig. 7(a) with X-ray mapping of alloying elements: Fig. 7(b) C, Fig. 7(c) Co and Fig. 7(d) Al. Note that cracks are seen as bright contrast in the carbon map in Fig. 7(b) because the specimen was mounted in a material containing carbon for electrical conductance. The WDS was used only for mapping of a light-element carbon. In the X-ray mapping, each constituent phase is easily differentiated. The B2 phase with a bright contrast can be easily distinguished from $E2_1$ phase especially in the aluminum map in Fig. 7(d). Several cracks are found to propagate through the B2 phase, and some of them go along its phase boundary as well. The eutectic microstructure consisting of $E2_1$/(Co) is supposed to provide considerable ductility of these alloy.

We may learn about the micro-crack initiation in the early stage of failure from a microstructure observation in the vicinity of the fracture surface. Our study clearly

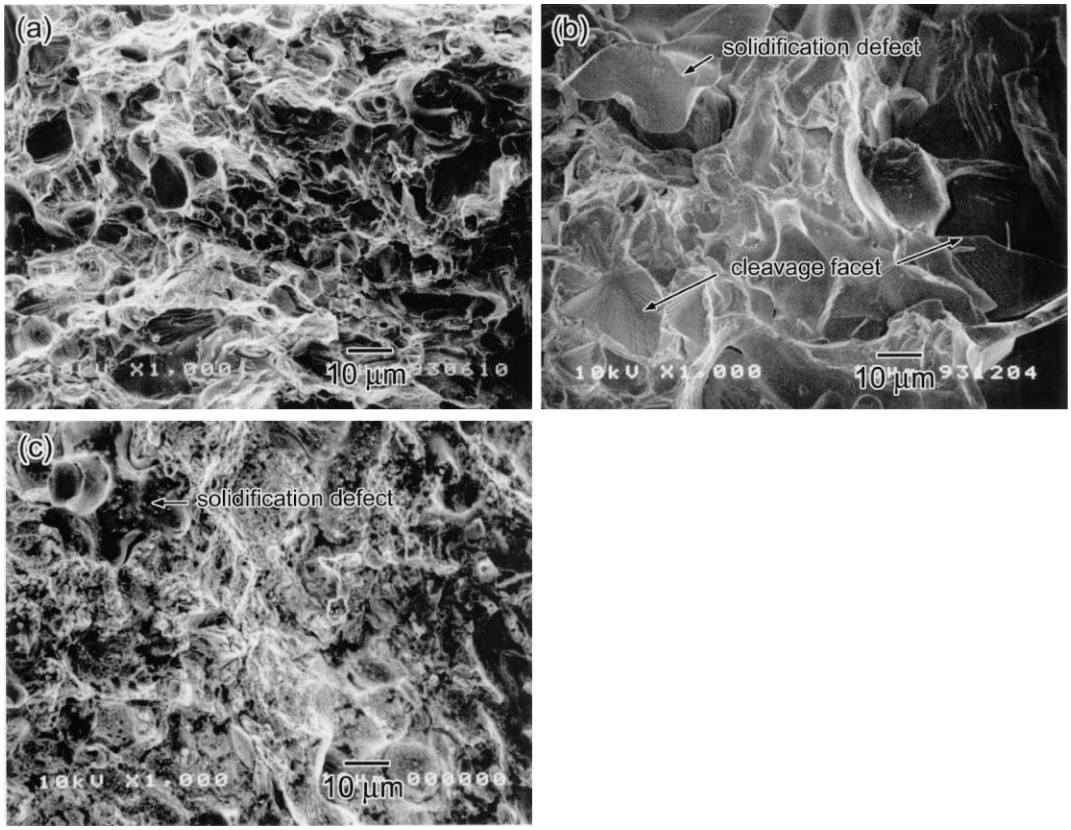

Fig. 6. Fractographs of as-annealed alloys: (a, c) alloy B, (b) alloy G, (a, b) at room temperature in air, and (c) at 1273 K in vacuum.

indicates that micro-cracks are always initiated at B2 particles due to the stress concentration, and then they are propagating through these particles. Eventually cracks would lead to a catastrophic failure by penetrating through the entire cross section of the specimen. Thus, the transgranular cleavage fracture at the $E2_1$ phase would not occur until the catastrophic crack propagation stage, i.e. the final stage of the failure. In other words, microcracking tends to initiate at the B2 phase but not take place at the $E2_1$ phase during the early stage of plastic deformation.

3.2. The effect of hot-forging combined with heat treatments

3.2.1. Microstructural modification

It is concluded from the previous section that solidification defects and coarse B2 phase particles are the cause of the limited ductility in the $E2_1$/B2/(Co) three-phase alloys. Thus, this microstructural heterogeneity has to be removed for the further improvement of mechanical properties. We performed hot forging combined with subsequent heat treatment on alloys B and G to improve ambient temperature ductility and toughness via microstructural control.

Modified microstructures are shown in Fig. 8(a)–(d). On comparison of as-forged microstructures shown in Fig. 8(a) for alloy B and Fig. 8(c) for alloy G with annealed cast microstructures shown in Fig. 4(a) and (b), the present hot forging condition, 50% reduction of thickness at 1373 K, seems to be effective enough in eliminating both solidification defects and as-cast microstructures. Relatively high residual strain is anticipated in the as-forged state. In fact, tensile tests conducted on as-forged specimens have revealed that the room temperature ductility can not be improved in the as-forged condition. This result indicates that a specific heat treatment is necessary to relieve residual strains introduced during hot forging. The microstructures of forged alloys B and G after the subsequent heat treatments (see Fig. 3) are shown in Fig. 8(b) and (d). As clearly seen in these micrographs, hot-forging combined with the heat treatments successfully diminishes the inhomogeneous morphology in cast alloys B and G.

3.2.2. Tensile mechanical properties improvement

To evaluate the effect of the microstructural control on the mechanical properties of alloys B and G, tensile tests were conducted at room temperature and at 1273 K. Stress–strain curves obtained from the tests are shown in Fig. 9. The results of all tensile tests are also summarized in Table 2 for as-annealed and modified alloys B and G, where $\sigma_{0.2}$ is 0.2% tensile flow stress, σ_{UTS} ultimate tensile strength, σ_f fracture stress, and ε_f fracture strain.

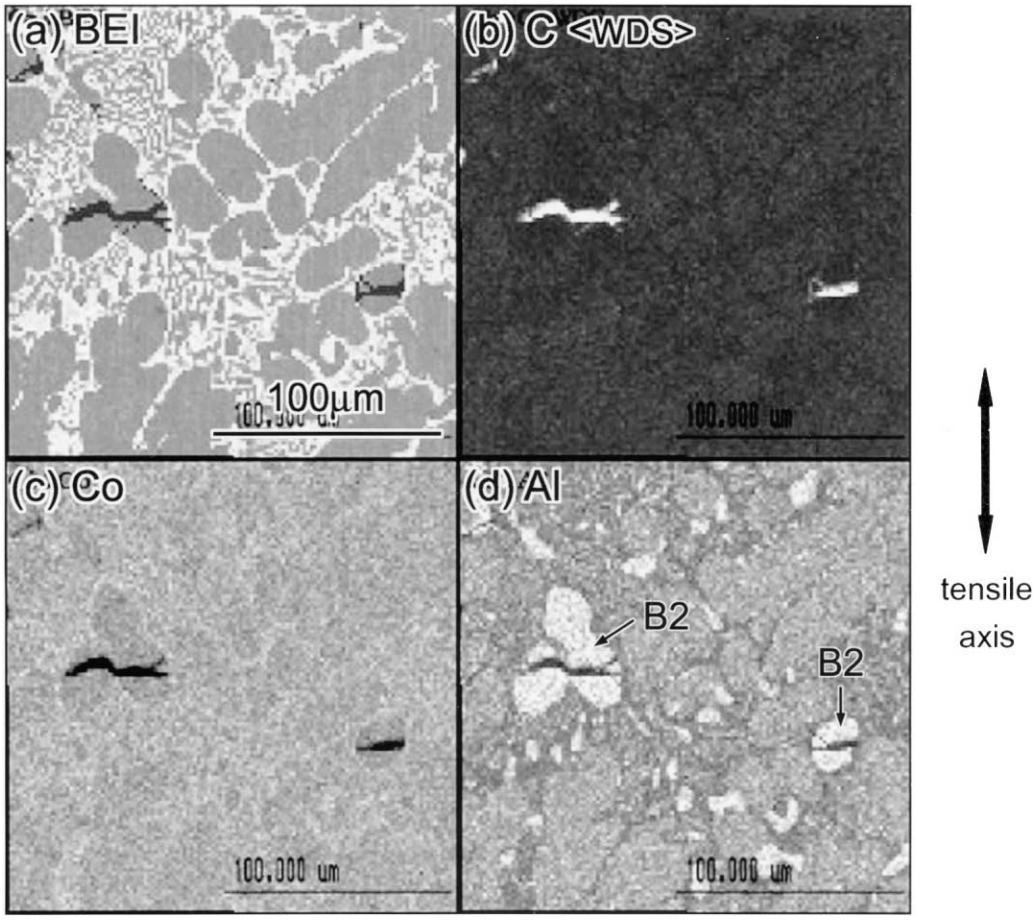

Fig. 7. A back-scattered electron image and X-ray mapping of each constitutive element for the side view of as-annealed alloy B tested at room temperature.

Hot forging combined with the specific heat treatments apparently improves the ambient temperature tensile ductility for both alloys B and G. The improvement is remarkable in the case of alloy G. The yield point is observed and 2.0% plastic deformation is achieved at room temperature in modified alloy G, while as-annealed cast alloy G fractures within the elastic region. However, the 0.2% tensile flow stress is about a half of that in compression, which indicates the ductility of alloy G is not yet fully improved. In the case of alloy B, good room temperature ductility (5.2%) is achieved in the as-annealed cast condition; however, modified alloy B exhibits further improvement in ductility reaching 8.6% strain after the microstructural control. Note that the stress-strain curve of modified alloy B at room temperature shows serrated flow after yielding. The serration is believed to be due to the propagation of Luders bands in well-annealed materials. Fig. 10 shows fractographs of modified alloys B and G tested at room temperature. There is no appreciable difference between the two fractographs, except large cleavage fracture facets of B2 phase in the modified alloy G due to its high volume fraction. No solidification defects are detected in the modified alloys.

The 0.2% flow stress and ultimate tensile strength at 1273 K is distinctly lower than those at room temperature in both modified alloys B and G. Whether the yield strength anomaly exists in tension is not confirmed by the present work, though both alloys B and G exhibit a positive temperature dependence of strength in compression, and alloy B has a two-step anomaly, as reported in the previous paper [19].

The temperature dependence of tensile ductility is quite different in the modified alloys B and G. The modified alloy B exhibits 7.5% plastic strain at 1273 K, which is almost the same at room temperature, while the modified alloy G shows much more ductility (18.9%) at 1273 K than that (2.0%) at room temperature. This propensity can be rationalized from the consideration of the volume fraction ratio of constituent phases. At room temperature, the modified alloy G, containing 30 vol.% B2, is much stronger but more brittle than the modified alloy B, containing 6 vol.% B2. The modified alloy G is more ductile at 1273 K, possibly because the B2 phase imparts plastic deformability in multi-phase alloys at elevated temperatures despite its brittleness at room temperature as reported previously [45].

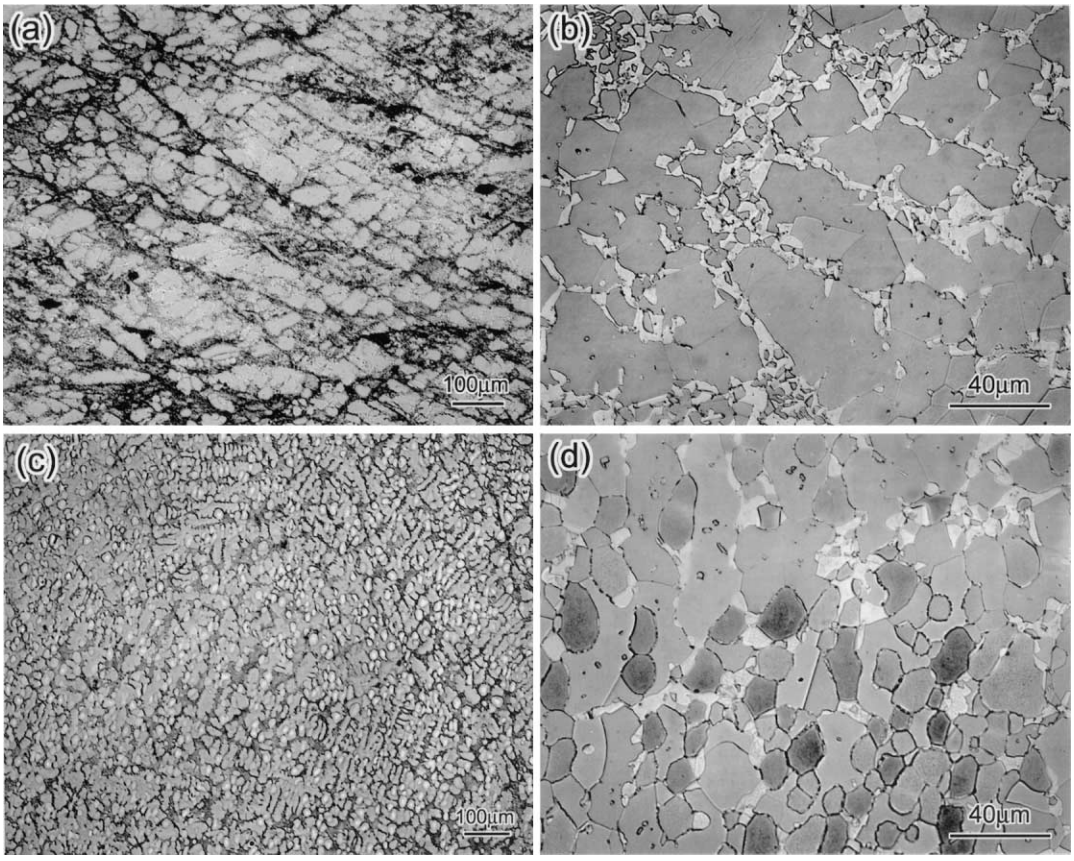

Fig. 8. Optical micrographs of alloys that experienced microstructure control: (a, b) alloy B, (c, d) alloy G, (a, c) as-forged microstructures, and (b, d) modified microstructures by hot-forging and subsequent heat treatment.

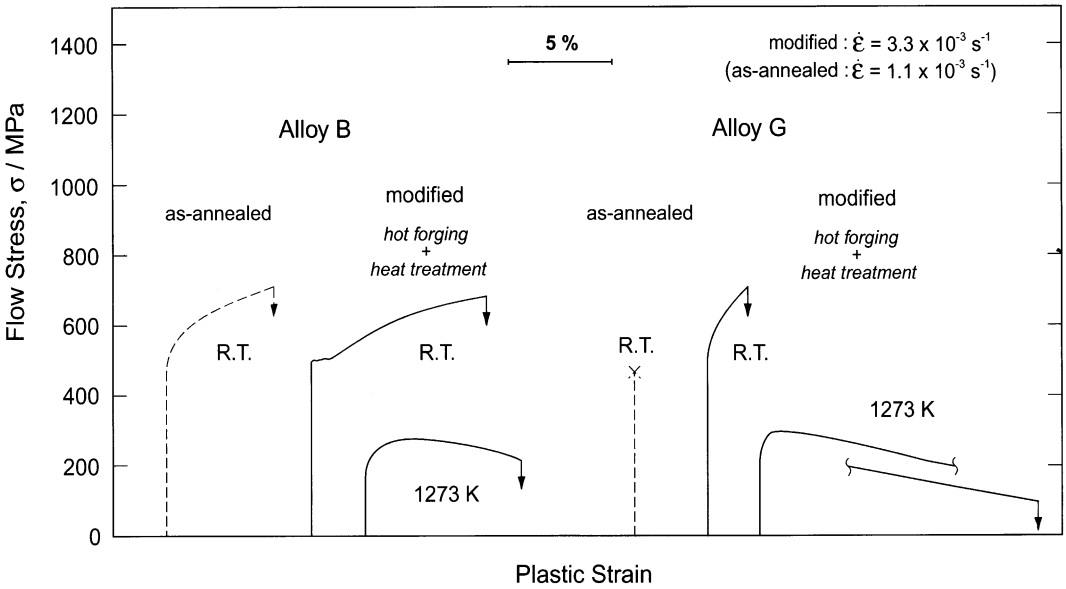

Fig. 9. Stress–strain curves of modified alloys B and G obtained from tensile tests at room temperature and at 1273 K.

3.3. Toughness considerations on multi-phase alloys

Generally, the plastic deformability of composite materials containing both a "brittle hard" phase and a "ductile soft" phase exhibits different mechanical behavior in compression and in tension [46,47]. In the case of the compression test, the "ductile soft" phase would compensate for the poor deformability of the "brittle hard" phase by imparting a considerable amount of plastic deformation. It enhances the overall apparent

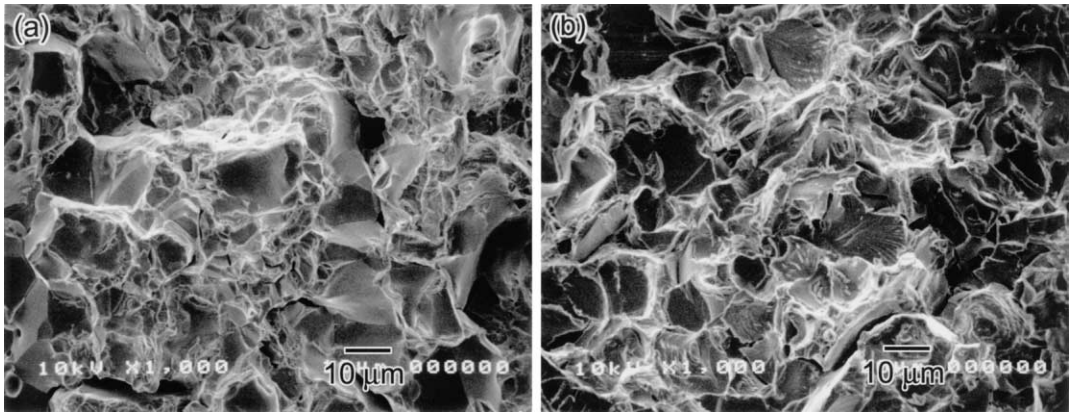

Fig. 10. Fractographs of modified alloys tested at room temperature: (a) alloy B, and (b) alloy G.

Table 2
Summary of tensile tests conducted on the $E2_1$/B2(Co) three-phase alloys B and G

Alloy	Temperature (K)	$\sigma_{0.2}$ (MPa)	σ_{UTS} or σ_f (MPa)	ε_f (%)
B	R.T.	463	712 (σ_f)	5.2
	1273	147	223 (σ_{UTS})	3.2
Modified B	R.T.	500	687(σ_f)	8.6
	1273	241	278 (σ_{UTS})	7.5
G	R.T.	–	469 (σ_f)	0
	1273	NA	NA	NA
Modified G	R.T.	566	668 (σ_f)	2.0
	1273	236	253 (σ_{UTS})	18.9

ductility of a material, and the ductility tends to be overestimated in compression. On the other hand, in the case of the tensile test, stress concentration occurs immediately at the "brittle hard" phase, and this leads to catastrophic failure such as cleavage fracture or separation at interfaces or grain boundaries. The fracture strength depends on the weakest point of a material such as solidification defects. If the fracture strength is lower than the yield strength, a material fractures before the onset of plastic deformation even though the material has a high plastic deformability in compression. As a consequence, the ductility is underestimated in tension. In this sense, tensile tests conducted on materials containing a "brittle hard" phase and/or solidification defects measure the fracture toughness instead of tensile mechanical behavior. This is the case of tensile test on as-annealed alloy G in the present work. To evaluate the potential of a material for structural applications at elevated temperatures, both compressive and tensile mechanical properties should be investigated over a wide temperature range.

One of characteristic microstructural features of alloy B is the absence of coarse B2 CoAl particles. This must be a desirable microstructure for both room temperature ductility and high temperature strength. Coarse dendritic structures are unfavorable for ductility. Consequently, for Co–Al–C ternary alloys with improved mechanical properties, finer and more homogeneous distribution of constituent phases is required. For this purpose, specific heat treatments combined with hot working promises an advantageous microstructural control to achieve improved mechanical properties of the alloys.

4. Conclusions

Mechanical properties of the $E2_1$/B2/(Co) three-phase alloys have been investigated at room temperature and 1273 K in tension for the purpose of the evaluation of their possibility as a new heat resistant structural material. Tensile tests were conducted on the selected alloys which showed excellent compressive room temperature ductility in the previous work. Hot forging combined with subsequent heat treatments has been used to improve ambient temperature ductility through microstructural control aimed at eliminating solidification defects and heterogeneity of the as-cast microstructure. The following conclusions are drawn from the present work.

1. Tensile tests on as-annealed cast alloys have revealed that alloy B, with a volume fraction of more than 50% $E2_1$ phase, exhibits a good room temperature tensile ductility of 5.2% plastic strain, while alloy G, with a volume fraction of about 30% B2 phase, shows zero plastic deformability even though it possesses virtually unlimited compressive ductility.

2. The microstructural modification achieved by hot forging and subsequent specific heat treatments effectively improves the ambient temperature ductility. Modified alloy B shows a good ductility of 8.6% as compared with 5.2% in the as-annealed cast condition. It is noteworthy to mention that the modified alloy G shows 2.0% plastic strain while the as-annealed cast alloy fractures within the elastic region.

3. The temperature dependence of ductility is quite different for modified alloys B and G. Alloy B shows good and comparable ductility at room temperature and at 1273 K, while alloy G is much more ductile at 1273 K than at room temperature.

4. A good balance of ductility and strength achieved in alloy B at room temperature and 1273 K indicates that the $E2_1$ Co_3AlC phase is an effective strengthener in Co-based heat resistant alloys.

Acknowledgements

The authors are deeply grateful to Ms. Claudette Mckamey for manuscript review and Mr. Elmer H. Lee at Oak Ridge National Laboratory his dedicated experimental assistance in the present work. This work was jointly supported by the Grant-in-Aid for Scientific Research from the Ministry of Education, Culture, Sports, Science and Technology of the Japanese Government under contract No.12305044, and the Division of Materials Science and Engineering, US Department of Energy under contract DE-AC05-00OR-22725 with UT-Battelle LLC.

References

[1] Mishima Y, Kato M, Kimura Y, Hosoda H, Miura S. Intermetallics 1996;4(Suppl. 1):s171.
[2] Kimura Y, Pope DP. In: Proc. intl. symp. on structural intermetallics, structural intermetallics 1997. Warrendale (PA): TMS, 1997. p. 99.
[3] In: Sims CT, Hagel WC, editors. The superalloys. New York: John Wiley & Sons, 1972.
[4] In: Sims CT, Stoloff NS, Hagel WC, editors. Superalloys II. New York: John Wiley & Sons, 1981.
[5] Ochiai S, Oya Y, Suzuki T. Acta Metall 1984;32:289.
[6] Suzuki T, Mishima Y, Miura S. ISIJ Intl 1989;29:1.
[7] In: Westbrook JH, Fleischer RL, editors. Intermetallic compounds, vol. 2, Practice. New York: John Wiley & Sons, 1995. p. 73.
[8] Yamaguchi M, Inui H, Kishida K, Matsumuro M, Shirai Y. In: High-temperature ordered intermetallic alloys VI, MRS Symp. Proc., vol. 364. Pittsburgh (PA): Mater. Res. Soc., 1995. p. 3.
[9] Yamaguchi M, Inui H, Ito K. Acta Mater 2000;48:307.
[10] Kimura Y, Suzuki T, Mishima Y. In: High-temperature ordered intermetallic alloys V, MRS Symp. Proc. vol. 288. Pittsburgh (PA): Mater. Res. Soc., 1993. p. 697.
[11] Kimura Y, Kuriyama H, Miura S, Suzuki T, Mishima Y. Mater Trans JIM 1994;35:182.
[12] Kimura Y, Miura S, Suzuki T, Mishima Y. In: Experimental methods of phase diagram determination. Materials Park (PA): TMS/ASM Symp Proc., 1993. p. 113.
[13] Kimura Y. Doctor thesis, Tokyo Inst. Tech., 1994.
[14] Kimura Y, Miura S, Suzuki T, Mishima Y. Mater Trans JIM 1994;35:800.
[15] Hosoda H, Takahashi M, Suzuki T, Mishima Y. In: High-temperature ordered intermetallic alloys VI, MRS Symp Proc., vol. 288. Pittsburgh (PA): Mater. Res. Soc., 1993. p. 793.
[16] Hosoda H. Doctor thesis, Tokyo Inst. Tech., 1993.
[17] Kimura Y, Takahashi M, Miura S, Suzuki T, Mishima Y. Intermetallics 1995;3:413.
[18] Kimura Y, Takahashi M, Miura S, Suzuki T, Mishima Y. In: High-temperature ordered intermetallic alloys VI, MRS Symp. Proc., vol. 364. Pittsburgh (PA): Mater. Res. Soc., 1995. p. 1371.
[19] Kimura Y, Takahashi M, Hosoda H, Miura S, Mishima Y. Intermetallics 2000;8:749.
[20] Huetter LJ, Stadelmaier HH, Fraker AC. Metall 1960;14:113.
[21] Grieb B, Stadelmaier HH. In: Petzow G, Effenberg G, editors. Ternary Alloys, vol. 4. Weinheim: VCH, 1991. p. 465.
[22] Singleton MF, Murray JL, Nash P. In: Massalski TB et al., editors. Binary phase diagrams, vol. 1, 2nd ed. Materials Park: ASM Intl., 1990. p. 181.
[23] Hwang KY. Doctor thesis, Tokyo Inst. Tech., 1998.
[24] Mishima Y, Hwang KY, Wei FG. In: High-temperature ordered intermetallic alloys VIII, vol. 552. MRS Symp Proc. 1999. p. KK.7.8.1.
[25] Hosoda H, Suzuki K, Hanada S. In: High-temperature ordered intermetallic alloys VIII, vol. 552. MRS Symp Proc., 1999. p. KK8.31.1.
[26] Nowotny H, Benesovsky F, In: Rudman PS et al., editors. Phase stability in metals and alloys. New York: McGraw Hill, 1967. p. 319.
[27] Stadelmaier HH, In: Giessen BC, editor. Developments in the structural chemistry of alloy phases. New York: Plenum Press, 1969. p. 141.
[28] Morral FRJ. Iron Steel Inst 1934;130:419.
[29] Nishida K. Technical reports of the Hokkaido University, 1968;48:71.
[30] Palm M, Inden G. Intermetallics 1995;3:443.
[31] Sanders W, Sauthoff G. Intermetallics 1997;5:361.
[32] Sanders W, Sauthoff G. Intermetallics 1997;5:377.
[33] Choo WK, Kim JH, Yoon JC. Acta Mater 1997;45:4877.
[34] Fahmy Y, Benfield CT, Koch CC. Mater Sci Eng A170 1993:19.
[35] von Philipsborn H, Laves F. Acta Crystallogr 1964;17:213.
[36] Tian WH, Sano T, Nemoto M. Phil Mag 1993;68:965.
[37] Pietzka MA, Schuster JC. J Am Ceram Soc 1996;79:2321.
[38] Kear BH, Wilsdorf HGF. Trans Met AIME 1962;224:382.
[39] Takeuchi S, Kuramoto E. Acta Metall 1973;21:415.
[40] Kuramoto E, Pope DP. Phil Mag 1976;34:593.
[41] Wee DM, Suzuki T. Trans JIM 1979;20:634.
[42] Wee DM, Noguchi O, Oya Y, Suzuki T. Trans JIM 1980; 21:237.
[43] Mishima Y, Oya Y, Suzuki T. Trans ISIJ 1985;25:1171.
[44] Miura S, Mishima Y, Suzuki T. Z Metallkde 1989;80:112.
[45] Mishima Y, Lee EH, Liu CT. Mater Trans JIM 1995;36:1031.
[46] Mishima Y, Miura S, Kimura Y. In: High-temperature intermetallics, ASM Intl. Symp. Proc., vol. A192/193. Materials Park: Mater. Sci. Eng., 1995. p. 748.
[47] Sigl LS, Mataga PA, Dalgleish BJ, McMeeking X, Evans AG. Acta Metall 1988;36:945.